NASA TN D-452

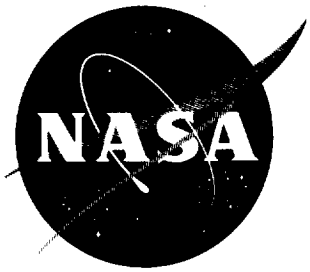

TECHNICAL NOTE
D-452

MODULATED ENTRY

By Frederick C. Grant

Langley Research Center
Langley Field, Va.

NATIONAL AERONAUTICS AND SPACE ADMINISTRATION
WASHINGTON
August 1960

NATIONAL AERONAUTICS AND SPACE ADMINISTRATION

TECHNICAL NOTE D-452

MODULATED ENTRY

By Frederick C. Grant

SUMMARY

The technique of modulation, or variable coefficients, is discussed and the analytical formulation is reviewed. Representative numerical results of the use of modulation are shown for the lifting and nonlifting cases. These results include the effects of modulation on peak acceleration, entry corridor, and heat absorption. Results are given for entry at satellite speed and escape speed. The indications are that coefficient modulation on a vehicle with good lifting capability offers the possibility of sizable loading reductions or, alternatively, wider corridors; thus, steep entries become practical from the loading standpoint. The amount of steepness depends on the acceptable heating penalty. The price of sizable fractions of the possible gains does not appear to be excessive.

INTRODUCTION

For low entry angles, provision of a small L/D is helpful in the reduction of peak loadings. At the higher entry angles, defined arbitrarily as those greater than 6°, even high L/D will not keep the peak loadings below some nominal limit such as 10g. For supercircular entry a g limitation defines a corridor width. To stay within a g limit at steep entry angles, the technique of modulation, or variable coefficients, must be introduced. In this paper numerical results will be shown only for entry at satellite and escape speed; however, the indicated trends are independent of the velocity.

In entry from escape speed, as in lunar return, the ability to withstand steep entry provides a margin for error in the guidance problem; however, at satellite speeds large retro-rockets are needed to achieve steep entry angles. From a practical standpoint there are certain military purposes, emergency conditions, and abort conditions for which it is possible that steep entry will be required at satellite speeds.

SYMBOLS

C_D	drag coefficient
C_L	lift coefficient
C_R	resultant-force coefficient
D	drag
g	acceleration due to gravity
h	altitude
$K = \frac{V_o^2}{2g\beta^{-1}}$	
L	lift
Q	total heat absorbed
r_B	ballistic modulation ratio
r_L	lifting modulation ratio
r_o	radius from center of earth to atmospheric entry point
V	velocity
x	horizontal distance
α	angle of attack
β^{-1}	atmospheric scale height, $-\frac{dh}{d \log_e \rho}$
γ	flight-path angle with local horizontal, positive up
Γ	minimum acceleration index
λ	parameter (ref. 1)
ρ	air density

Subscripts:

MAX	maximum
MIN	minimum
Mod	modulated
o	initial conditions
Opt	optimum
pe	perigee
Unmod	unmodulated
1	start of modulation
2	end of modulation

A dot over a symbol indicates a derivative with respect to time. Bar over symbol indicates values for $(L/D)_{MAX}$.

DISCUSSION

The modulation principle is illustrated in figure 1 which shows a loading history with and without modulation for a lifting vehicle. The resultant aerodynamic force in units of the vehicle weight is plotted against the corresponding times. In the upper right corner, the corresponding trajectories are sketched. For the unmodulated case, the loading rises to a sharp peak just before the bottom of the pull-up at which point the curve has been ended (corresponds to the upper trajectory in the sketch). For the modulated case, at some point in the entry the loading is not allowed to increase further and is held constant by continuous reduction of the resultant-force coefficient (corresponds to the lower trajectory in the sketch). Deeper penetrations of the atmosphere always occur in modulated pull-ups. If the proper point for start of the modulation has been selected, the vehicle will have nearly zero lift coefficient as it levels out. If the modulation is started too soon, the vehicle will not have leveled out sufficiently as the lift coefficient approaches zero. Higher loadings will be experienced subsequently than were maintained during the modulation period. For late starts of the modulation and consequent higher loading levels, the lift coefficient will not have approached zero at the bottom of the pull-up and the full capability of the vehicle will not be realized. For the

case shown, the shaded area next to the unmodulated curve may be loosely regarded as an impulse which is shifted to later times and lower loading levels for the modulated case. For precision, components of the impulse must be considered. The basic idea, however, is to replace a large force acting for a short time by a smaller force acting for a longer time to make essentially the same change in velocity. The modulation scheme indicated in figure 1 is that used in references 1 and 2.

The following simple relation governs the air loading:

$$\frac{\text{Resultant force}}{\text{Weight}} \propto C_R \rho V^2$$

As indicated in figure 1 the rise in ρV^2 during entry is combated during the modulation period by the decrease in C_R. The following two cases can be distinguished:

Ballistic:

$$C_R = C_D$$

Lifting:

$$C_R = \sqrt{C_D^2 + C_L^2}$$

In the ballistic case the drag coefficient is reduced during modulation. In the more complicated lifting case both lift and drag coefficients are changed simultaneously according to whatever functional relation exists between them.

The nature of the difference between the two cases can be visualized more concretely in terms of force polars. Force polars for the two cases are sketched in figure 2 along with the physical means necessary to attain the polars. In the ballistic case an axisymmetric vehicle is visualized as decreasing its frontal area from a large value to a small value. The corresponding polar is part of the C_D axis. In the lifting case a winged vehicle is visualized as changing attitude from an angle of attack of 90° to an angle of attack of 0° while the force coefficients trace out a loop in the C_D, C_L plane. This is the extreme range of lift modulation; the optimum range lies, as will be shown, between maximum lift coefficient and minimum drag coefficient.

In the ballistic case a geometry modulation is needed; in the lifting case an attitude modulation is needed. Other cases can be imagined in which both geometry and attitude modulation occur simultaneously and thus

trace out paths intermediate to the two shown. It can be shown (refs. 3 and 4) that the g-alleviation capability for the lifting case depends strongly on a single parameter, the maximum lift coefficient in units of the minimum drag coefficient. For the ballistic case, the alleviation depends on the ratio of maximum drag coefficient to minimum drag coefficient. (See ref. 1.) For unit minimum drag coefficient the parameters appropriate to the two cases are marked on the polars as r_B, the ballistic modulation ratio, and r_L, the lifting modulation ratio. In the analysis of reference 2, the modulation was effectively restricted to the portion of the polar on the low-drag side of maximum lift-drag ratio (between the two lowest dots). This restriction leads to an underestimation of the possible g alleviation and an overestimation of the heat load associated with a given g level.

L
1
0
4
9

ANALYTICAL FORMULATION

Isolation of the two modulation parameters is made possible by the separation of the modulation problem into two limiting cases with appropriate analytic assumptions. (See fig. 3.) Formulas derived with these assumptions are presented in appendix A. In the ballistic case variations in the flight-path angle are presumed to be unimportant whereas the velocity changes are considered to be significant. In the lifting case the complementary assumptions are made; that is, changes in velocity are ignored whereas changes in flight-path angle are considered to be important. In physical terms, the assumptions correspond to separation of the two possible operations on the velocity vector, changes of magnitude and changes of direction. On course, these assumptions do not apply to the portions of the trajectories beyond peak g which are indicated in figure 3 as dashed lines.

The assumption of constant velocity in the lifting case is conservative in the sense that it leads to an underestimation of the g alleviation. Neglect of the actual velocity decrease means that in the real lifting case higher lift coefficients can be used at the same altitudes for the same loading limit. A lower loading limit than is indicated by the analysis is thus possible in the real case.

The ballistic case has been analyzed in reference 1 and the principal result is indicated in figure 4. Plotted vertically is the peak resultant force in units of the peak resultant force for no modulation. The sole parameter on which the g alleviation depends is the modulation ratio r_B, the ratio of maximum drag to minimum drag. A region of rapid initial gains is followed by one in which diminishing returns have set in. The alleviation ratio always decreases but always at a slower rate. The ballistic case is completely solved in terms of the ballistic

modulation ratio. In the lifting case, a different modulation ratio, maximum lift coefficient to minimum drag coefficient, plays the leading role.

The analysis of the lifting case (refs. 2 to 4) is complicated by the simultaneous appearance of lift and drag coefficients. The principal result of the analysis is shown in figure 5. The vehicle is presumed to enter the atmosphere at some specified lift and drag coefficients indicated as point 1 on the schematic polar at the upper left. At some point in the trajectory, shown at the right, the resultant force is held constant and the coefficients are varied through the bottom of the pull-up (point 2) and trace a portion of the drag polar from points 1 to 2. For this type of entry, the loading that is held during the modulation along arc 1,2 is found to vary inversely with a function Γ. (See fig. 5.) The integral term of this function is the more important and is a simple line integral along the polar. Since the peak loading is minimum for maximum Γ, it is of interest to know the proper choice of points 1 and 2 which yields maximum Γ for any given polar. By differentiation of the Γ function, the maximum value of Γ is found to occur for modulation between maximum lift coefficient and minimum drag coefficient.

The optimum polar with which to connect specified maximum lift and minimum drag points is indicated in figure 6 and is derived as follows: Since the endpoints are specified, it is a question of maximizing the integral term (fig. 6) of the function Γ. Since the integration is with respect to C_R, the largest possible C_L at every C_R value is required. Lines of constant C_R are circles centered on the origin, one of which is indicated in the figure. The dashed curve (fig. 6) represents a realistic polar between points 1 and 2. For maximum C_L at a given C_R, the dashed curve must be pushed as far clockwise as possible along the lines of constant C_R. This movement forces the dashed curve into coincidence with the right-angle polar between points 1 and 2 (drawn as a solid line). For the right-angle polar, Γ is a simple logarithmic function only of the ratio of maximum lift coefficient to minimum drag coefficient. The values of Γ for real polars will be somewhat less than the values for right-angle polars between the same maximum lift and minimum drag points. However, the previously mentioned conservative nature of the constant-velocity assumption leads in many cases to better loading estimates when the right-angle polar is substituted for the actual polar.

For a family of vehicles with Newtonian drag polars, the results of the lifting analysis are shown in figure 7. The base loading is, in this case, that experienced in entry at the corner of the optimum polar. (See appendix B.) Although the analysis yields results in terms of the

lift modulation parameter, in this figure the corresponding $(L/D)_{MAX}$ of the vehicle has been used. Since vehicles of increasing $(L/D)_{MAX}$ have increasing lift-modulation parameters, the trend of the curves is the same on either basis. As in the ballistic case, diminishing returns appear at the higher parameter values, but appreciable gains are evident for $(L/D)_{MAX}$ values as low as unity. The ratios plotted in figure 7 are independent of the velocity and entry angle to the order of approximation of the analysis.

L
1
0
4
9

NUMERICAL RESULTS

Figure 8 shows some concrete examples of the acceleration levels to be expected for steep entry at satellite speed with and without modulation. (See appendix A.) The entry-angle range is between 6° and 12°. On the left are shown the unmodulated g levels for the ballistic case, $L/D = 0$, and for a pure lifting case, $L/D = \infty$. Curves for the higher finite L/D values cluster in the neighborhood of the $L/D = \infty$ curve. With a nominal limit of 10g only the lifting vehicle at the low end of the range is acceptable. In the modulated case it is necessary to put limitations on the modulation capability. For example, in the ballistic case, an indefinitely large modulation capability means indefinitely low peak loadings. A vehicle which had and used such a capability would strike the earth just as if the earth had no atmosphere. Similar considerations preclude an infinite modulation ratio in the lifting case. For the ballistic case, then, a 50-to-1 drag-modulation capability was assumed as a representative high value. For the lifting case an L/D of 2 was specified as representing a high lift capability. On the basis of 10g being permissible, the ballistic vehicle is acceptable through most of the range and the lifting vehicle is satisfactory through the entire range. For escape speed the absolute values of the loadings are different, but the relative magnitudes are about the same.

Until now nothing has been said about the effect of modulation on entry corridor width or on the heating penalties associated with modulated entry. Figure 9 deals with these considerations. (See appendix C.) The vertical scale is Chapman's entry corridor width in miles for a 10g entry at escape velocity; the horizontal scale is the $(L/D)_{MAX}$ of a family of vehicles with Newtonian drag polars. Two modes of operation are indicated by solid lines: full modulation from maximum lift coefficient and no modulation from maximum lift-drag ratio. Rather spectacular gains in corridor width are evident for the higher L/D, at least in terms of the $L/D = 0$ value which is about 7 miles. Some idea of the relative heating penalties is indicated for a vehicle with the high L/D of 2.8. This represents a difficult case. Vehicles of lower $(L/D)_{MAX}$ will have easier heating problems.

Trajectories corresponding to the four modes of operation of the high L/D vehicle are indicated in figure 10. The dashed portions of the trajectories indicate the portions corresponding to the modulation period. Note that all the pull-ups are completed within a minute. The reference total heat is that absorbed down to the bottom of the pull-up for entry at maximum lift coefficient without modulation. Figure 10 shows this to be the highest altitude lowest heating pull-up and figure 9 shows it to have the narrowest corridor. Entry at $(L/D)_{MAX}$ without modulation yields a wider corridor but 2.3 times as much heat absorption. Passing to full modulation yields the widest corridor, the deepest penetration, and 6.1 times as much heat absorbed. The remaining trajectory corresponds to partial utilization of the vehicle capability. For this case more than 100 miles of corridor can be maintained for 1.7 times as much heat absorption as in the narrow-corridor low-heating pull-up at maximum lift coefficient without modulation. In terms of weight, this means about 70 percent more ablative material is required. In general, the question comes down to a trade-off between corridor width and heating penalties and can be settled only by a systems study of the mission. Since modulation from maximum lift coefficient is more favorable from both the heat absorption and loading standpoints, it is merely a question of how far to modulate.

Results for drag modulation on a ballistic vehicle are not shown in figure 9 since the gains are small. At $r_B = 21$, calculations have shown the ballistic vehicle to gain in corridor width from 7 to 30 miles while heat absorption rises about 60 percent. The unit of heat absorption is, of course, different from that used in the lifting example just discussed.

In figure 10, the peak heating rates in the pull-ups range from about 500 Btu/ft^2-sec in the pull-up at $(C_L)_{MAX}$ without modulation to about 2,800 Btu/ft^2-sec in the pull-up with full modulation. All the heating values shown in figures 9 and 10 refer to the stagnation point of a 1-foot-radius sphere at which point the heating rate is presumed to vary as $\rho^{1/2}V^{3.15}$.

CONCLUDING REMARKS

In conclusion, it may be said that coefficient modulation on a vehicle with good lifting capability offers the possibility of sizable loading reductions or, alternatively, wider corridors so that steep entries become practical from the loading standpoint. The amount of steepness depends on the heating penalty that is acceptable; however, the price of sizable fractions of the total possible gains does not appear to be excessive.

Langley Research Center,
National Aeronautics and Space Administration,
Langley Field, Va., April 11, 1960.

APPENDIX A

FORMULAS DERIVED BY USE OF ANALYTIC ASSUMPTIONS

The analytic assumptions indicated in figure 3 have allowed a number of simple peak loading formulas to be derived. These formulas are:[1]

Unmodulated ballistic (ref. 5):

$$\frac{\text{Resultant force}}{\text{Weight}} = -\frac{\sin \gamma_o}{e} K$$

Unmodulated lifting (ref. 2):

$$\frac{\text{Resultant force}}{\text{Weight}} = 2(1 - \cos \gamma_o)\sqrt{1 + \left(\frac{D}{L}\right)^2}\, K \qquad \text{(A1a)}$$

Modulated ballistic (ref. 1):

$$\frac{\text{Resultant force}}{\text{Weight}} = -\frac{\sin \gamma_o}{e} \lambda e^{1-\lambda} K$$

$$r_B = \lambda e^{\frac{1}{\lambda} - 1} \qquad (0 \leq \lambda \leq 1)$$

Modulated lifting (ref. 3):

$$\frac{\text{Resultant force}}{\text{Weight}} = \frac{2(1 - \cos \gamma_o)K}{\Gamma} \qquad \text{(A1b)}$$

$$\Gamma = \sinh^{-1} r_L \quad \text{(for ideal polars)}$$

The additional assumption that the net force due to gravity and coordinate acceleration is a small fraction of the aerodynamic force is implied by these formulas. Details are given in the indicated references.

---

[1]Differences of notation from that of the references have been introduced. In the case of reference 2 a factor accounting for velocity decrement has been suppressed to conform with the constant-velocity assumption.

The quantity K is the constant acceleration in g units required to absorb the initial kinetic energy during straight line motion over a length equal to the scale height β^{-1}; that is,

$$K = \frac{V_o^2}{2g\beta^{-1}}$$

The formulas (A1) above have been used to plot figure 8. In figure 8 the parameter values assumed are: V_o = 25,900 fps; β^{-1} = 23,300 ft; and g = 32.2 fps.

APPENDIX B

DETAILS OF CALCULATIONS OF ALLEVIATION FUNCTION IN LIFTING CASE

For attitude modulation on a vehicle with an ideal polar (fig. 6) the minimum peak loading has been shown to be (ref. 3)

$$\left(\frac{\text{Resultant force}}{\text{Weight}}\right)_{\text{Mod}} = \frac{V_o^2}{2g\beta^{-1}} \frac{2(1 - \cos \gamma_o)}{\Gamma_{\text{Opt}}} \tag{B1a}$$

where

$$\Gamma_{\text{Opt}} = \sinh^{-1} r_L \tag{B1b}$$

The corresponding peak loading for entry without modulation (at the corner of the ideal polar) is (from appendix A)

$$\left(\frac{\text{Resultant force}}{\text{Weight}}\right)_{\text{Unmod}} = \frac{V_o^2}{2g\beta^{-1}} \frac{2(1 - \cos \gamma_o)}{\frac{r_L}{\sqrt{1 + r_L^2}}} \tag{B2}$$

The alleviation ratio shown in figure 7 is the quotient of equations (B1) and (B2); that is,

$$\frac{\text{Modulated resultant force}}{\text{Unmodulated resultant force}} = \frac{r_L}{\sqrt{1 + r_L^2}\, \sinh^{-1} r_L} \tag{B3}$$

The Newtonian drag polars of reference 6 have been used to provide the relation between r_L and $(L/D)_{MAX}$ which is implicit in figure 7. These polars may be written in the form

$$\left.\begin{aligned} C_L &= C_{D_{MAX}}\left(1 - \frac{1}{r_B}\right)\sin^2\alpha \cos \alpha \\ C_D &= C_{D_{MAX}}\left[\frac{1}{r_B} + \left(1 - \frac{1}{r_B}\right)\sin^3\alpha\right] \end{aligned}\right\} \tag{B4a}$$

The angle for maximum lift coefficient is $\tan^{-1}\sqrt{2}$ and that for maximum lift-drag ratio $\bar{\alpha}$ is defined by the relation

$$\left(\frac{L}{D}\right)_{MAX} = \frac{1 + 3\cos 2\bar{\alpha}}{3\sin 2\bar{\alpha}} \qquad \text{(B4b)}$$

The corresponding ratio r_B of maximum drag to minimum drag on the polar is found from the relation

$$\frac{2}{r_B - 1} = \frac{3\sin\bar{\alpha} - \sin 3\bar{\alpha}}{1 + 3\cos 2\bar{\alpha}} \qquad \text{(B4c)}$$

The relation between r_B and r_L for the polars (B4a) is

$$r_L = \frac{2\sqrt{3}}{9}(r_B - 1) \qquad \text{(B4d)}$$

Eliminating r_B between equations (B4c) and (B4d) yields r_L as a function of $\bar{\alpha}$ and hence through equation (B4b), of $(L/D)_{MAX}$.

Although figure 7 shows a correct trend, proper use of the numerical values requires that the basis of the figure be clearly understood. The Γ values used in figure 7 are those corresponding to optimum polars between the maximum lift and minimum drag points of the polars given in eq. (B4a). Also, the unmodulated peak loading (the unit loading) is that experienced in an entry for which $L/D = r_L$. Thus, at the higher L/D values, the reference loading is essentially that experienced without modulation at infinite L/D. The ratios of figure 7 can be scaled to whatever values of Γ and $\left(\frac{\text{Resultant force}}{\text{Weight}}\right)_{\text{Unmod}}$ are appropriate by the relations

$$\left.\begin{aligned}\left(\frac{\text{Resultant force}}{\text{Weight}}\right)_{\text{Mod}} &\propto \frac{1}{\Gamma} \\ \left(\frac{\text{Resultant force}}{\text{Weight}}\right)_{\text{Unmod}} &\propto \sqrt{1 + \left(\frac{D}{L}\right)^2}\end{aligned}\right\} \qquad \text{(B5)}$$

APPENDIX C

DETAILS OF CALCULATIONS OF CORRIDOR WIDTH

The curves and points of figure 9 correspond either to numerical integrations or to formulas such as those used to construct figure 8. To avoid confusion, the construction of figure 9 requires explanation.

The conic perigee point for the undershot boundary was determined in all cases by the relation:

$$(r_o - r_{pe})_{undershoot} = r_o \sin^2(\gamma_o)_{MAX} \qquad (C1)$$

which holds for parabolic orbits. The values of $(\gamma_o)_{MAX}$ corresponding to a given load limit (10g in fig. 9) were determined either by the formulas of appendix A or by numerical integrations.

The overshoot boundary was defined as the altitude at which $C_{L_{MAX}}$ in inverted flight yields 1 g unit of aerodynamic lift. This definition is consistent with the assumption of constant velocity. The actual overshoot boundary is somewhat higher.

The values of stagnation-point relative heat shown in figure 9 and the corresponding corridor widths were all obtained by numerical integration in the ARDC atmosphere (ref. 7) for the $L/D = 2.8$ vehicle of references 3 and 4. For this vehicle $(r_o - r_{pe})_{overshoot} \approx (0.10)10^6$ feet. The initial conditions were $V_o = 36{,}500$ feet per second at $h_o = 350{,}000$ feet. The curve marked unmodulated was faired to agree with the machine computations for this vehicle. Results from references 6 and 8 lie slightly below this curve. The trajectories of figure 10 were obtained in the same numerical integration which yielded the heating values.

The curve marked "full modulation" is based on the alleviation function indicated in figure 7 and explained in appendix B.

REFERENCES

1. Phillips, Richard L., and Cohen, Clarence B.: Use of Drag Modulation to Reduce Deceleration Loads During Atmospheric Entry. ARS Jour., vol. 29, no. 6, June 1959, pp. 414-422.

2. Lees, Lester, Hartwig, Frederic W., and Cohen, Clarence B.: The Use of Aerodynamic Lift During Entry Into the Earth's Atmosphere. GM-TR-0165-00519, Space Tech. Labs., Inc., Nov. 20, 1958.

3. Grant, Frederick C.: Importance of the Variation of Drag With Lift in Minimization of Satellite Entry Acceleration. NASA TN D-120, 1959.

4. Grant, Frederick C.: Analysis of Low-Acceleration Lifting Entry From Escape Speed. NASA TN D-249, 1960.

5. Allen, H. Julian, and Eggers, A. J., Jr.: A Study of the Motion and Aerodynamic Heating of Ballistic Missiles Entering the Earth's Atmosphere at High Supersonic Speeds. NACA Rep. 1381, 1958. (Supersedes NACA TN 4047.)

6. Chapman, Dean R.: An Analysis of the Corridor and Guidance Requirements for Supercircular Entry Into Planetary Atmospheres. NASA TR R-55, 1959.

7. Minzner, R. A., and Ripley, W. S.: The ARDC Model Atmosphere, 1956. Air Force Surveys in Geophysics No. 86 (AFCRC TN-56-204), Geophysics Res. Dir., AF Cambridge Res. Center (Bedford, Mass.), Dec. 1956. (Available as ASTIA Doc. 110233.)

8. Chapman, Dean R.: An Approximate Analytical Method for Studying Entry Into Planetary Atmospheres. NASA TR R-11, 1959. (Supersedes NACA TN 4276.)

MODULATION PRINCIPLE

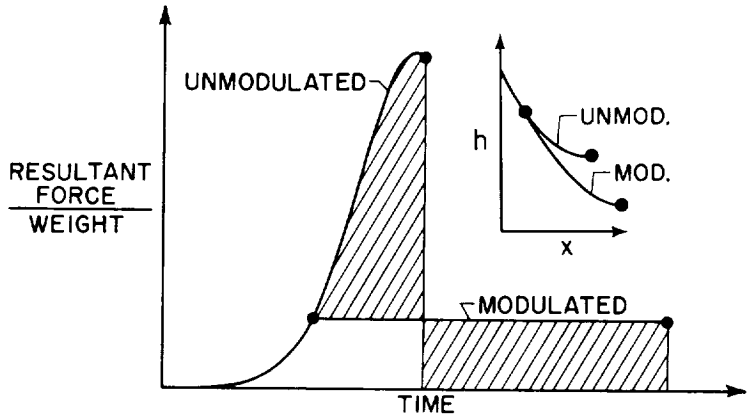

Figure 1

GEOMETRY AND ATTITUDE MODULATION

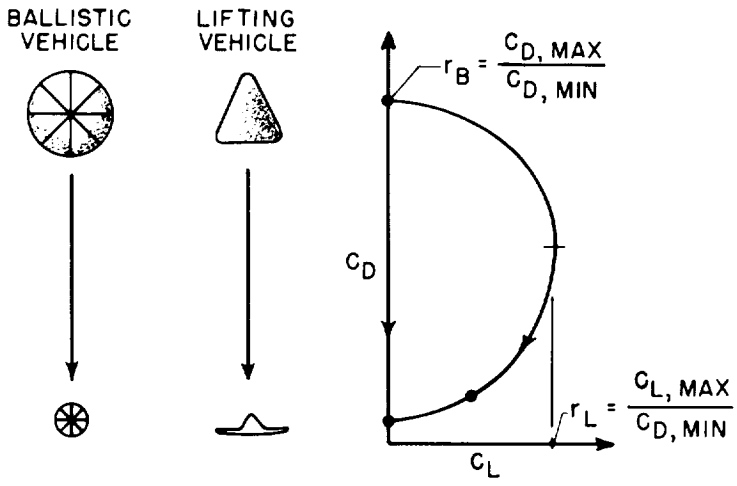

Figure 2

ANALYTIC ASSUMPTIONS

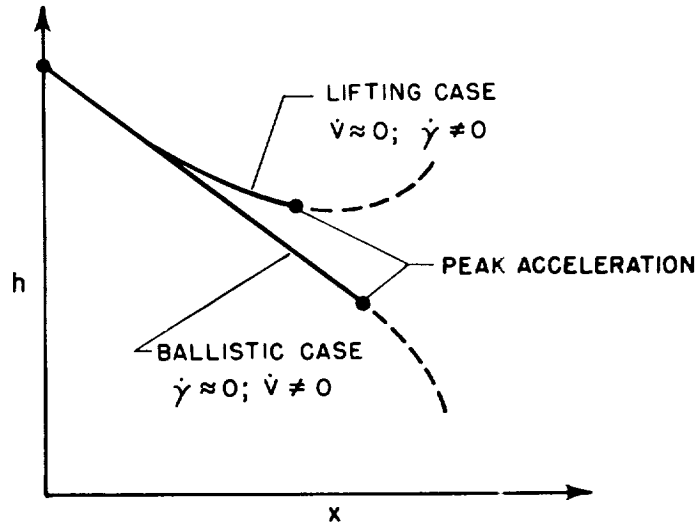

Figure 3

BALLISTIC-CASE GEOMETRY MODULATION

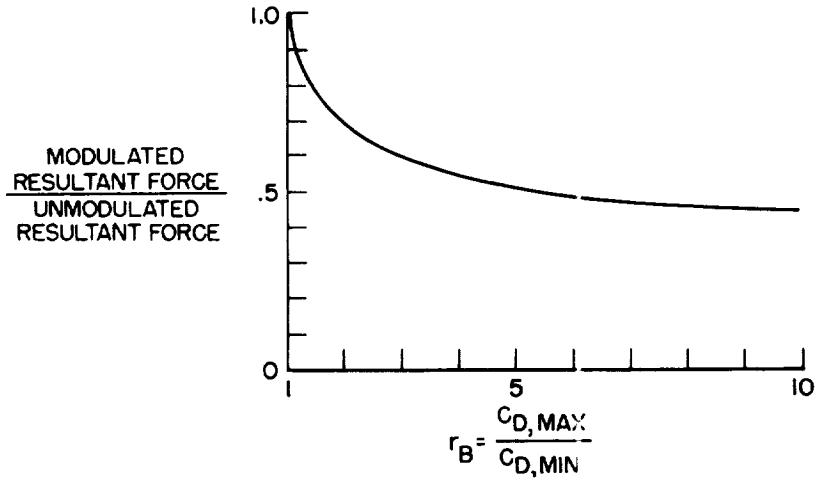

Figure 4

LIFTING-CASE ANALYTICAL RESULTS

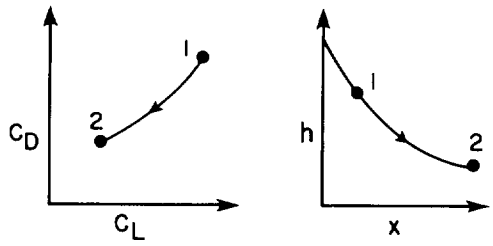

$$\left(\frac{\text{RESULTANT FORCE}}{\text{WEIGHT}}\right)_{MAX} \propto \frac{1}{\Gamma_{12}}$$

$$\Gamma_{12} = \left(\frac{C_L}{C_R}\right)_1 + \int_2^1 \frac{C_L}{C_R}\, d\ LOG_e\ C_R$$

Figure 5

LIFTING-CASE OPTIMUM POLAR

$$\int_2^1 \frac{C_L}{C_R}\, d\ LOG_e\ C_R$$

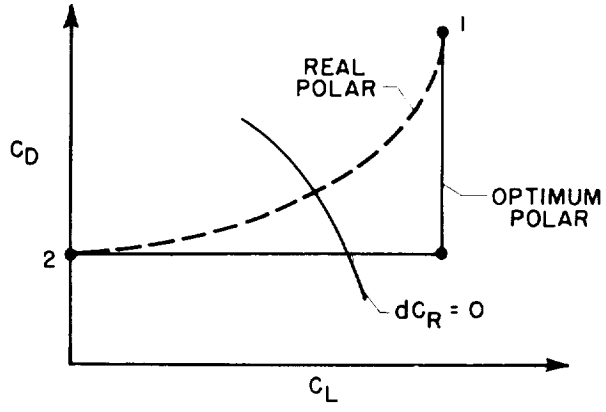

Figure 6

LIFTING-CASE ATTITUDE MODULATION

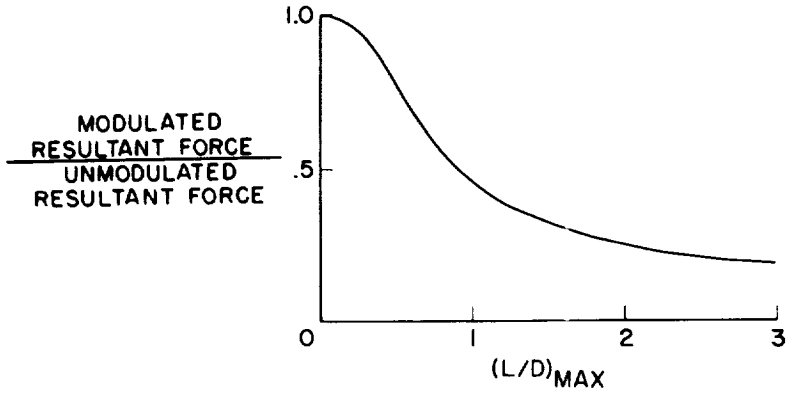

Figure 7

PEAK ACCELERATIONS

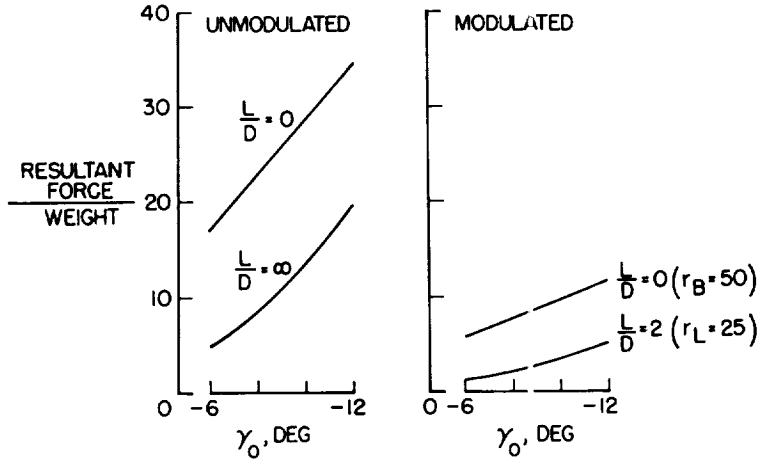

Figure 8

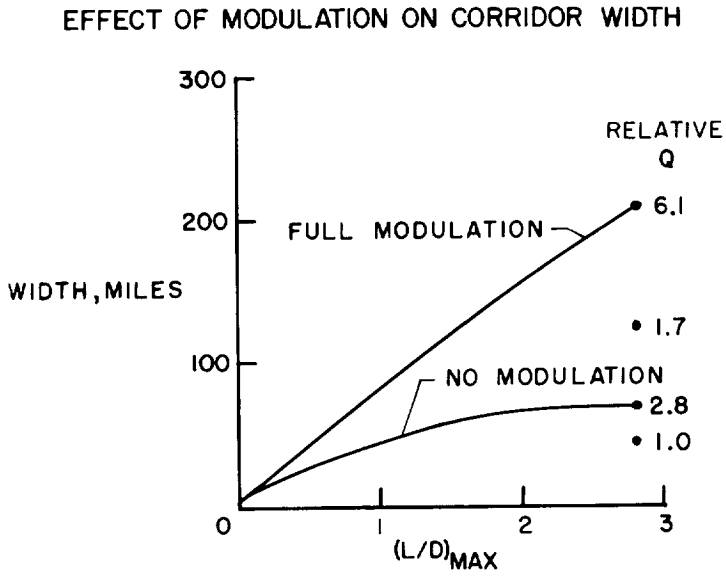

Figure 9

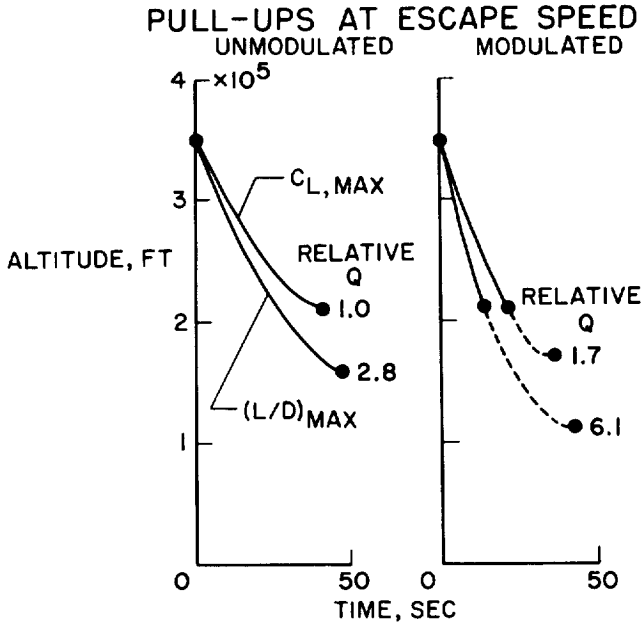

Figure 10

L-1049